Journal of Manufacturing Processes 162 (2026) 139–149

Contents lists available at ScienceDirect

Journal of Manufacturing Processes

journal homepage: www.elsevier.com/locate/manpro

Low-cost thermal reshaping of carbon fibre/PEEK thick sections: Experiments and simulations

Antreas Potsis [a], Fernando Álvarez-Borges [b], Irene Jiménez-Fortunato [c], Erick Montes de Oca Valle [c], Francisca Martínez-Hergueta [a,*]

[a] School of Engineering, Institute of Infrastructure and Environment, The University of Edinburgh, Sanderson Building, Robert Stevenson Road, Edinburgh, EH9 3FB, Scotland, United Kingdom
[b] μ-VIS X-ray Imaging Centre, School of Engineering, Faculty of Engineering and Physical Sciences, University of Southampton, University Road, Southampton, SO17 1BJ, United Kingdom
[c] Magma Global Ltd. Magma House, Trafalgar Wharf, Hamilton Road, Portsmouth, PO6 4PX, United Kingdom

HIGHLIGHTS

- A tool-free, low-energy thermal reshaping method is developed experimentally and numerically.
- Thick CF/PEEK pipes are processed for the first time at temperatures well below the melting point.
- Flatness is improved by up to 65% at relatively low pressures.
- Micro CT inspection shows that void content can be regulated by the applied pressure.
- This study paves the way for new methods in industrial waste management.

GRAPHICAL ABSTRACT

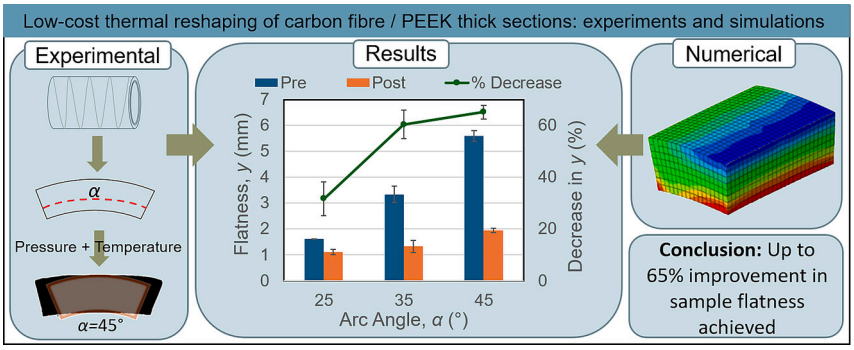

ARTICLE INFO

Keywords:
CF/PEEK
Thermal reshaping
Micro CT
Finite element modelling
Tape placement

ABSTRACT

This study develops a new low-cost remoulding route to reshape thick composite waste. A coupled experimental and numerical methodology is proposed and applied to carbon fibre polyether ether ketone pipes from oil and gas industry. The experimental procedure concludes that sample flatness can be improved by up to 65% without using additional moulds and for relatively low pressures and processing temperatures, above the glass transition temperature but well below the material's melting point, minimising the energy consumption and cost of the process. Micro CT inspection reveals a significant reduction in local void content in regions subjected to transverse compression, ensuring the quality of the reshaped component. The capabilities and limitations of different processing parameters are assessed numerically. Guidelines for sustainable reshaping of composite waste for different applications are provided, opening the path for a new method of managing composite waste at a minimum cost.

* Corresponding author.
E-mail address: Francisca.mhergueta@ed.ac.uk (F. Martínez-Hergueta).

https://doi.org/10.1016/j.jmapro.2026.02.002
Received 16 September 2025; Received in revised form 4 December 2025; Accepted 1 February 2026
Available online 12 February 2026

1. Introduction

Over the past decades, composite materials have systematically replaced metals and ceramics in various industries, due to their superior performance of specific mechanical properties [1]. Examples include aerospace [2], oil and gas [3] and automotive [4] industries. These superior properties, coupled with technological advancements and innovative manufacturing processes, especially of larger and more complex geometries, are enabling the exponential growth of composite production [5]. However, this expected growth will lead to an increase in composite waste, either from offcut pieces during manufacturing, or due to decommissioning [6]. It is therefore necessary to repurpose such waste and recycle end-of-life products to coincide with governmental net-zero targets [7].

Composite products may be produced from either thermoset or thermoplastic resins. The market is currently dominated by thermoset composites, which present several difficulties for recycling due to the need for high-temperature treatments or hazardous chemicals with a high cost and environmental impact [8–10]. On the other hand, thermoplastic composites may be thermally reshaped, allowing components to be repurposed and recycled at a reduced cost and carbon footprint [11,12]. Thermal reshaping is the manufacturing process in which a part is permanently deformed by being heated above the material's glass transition temperature and pressed into a mould [13]. It is an attractive manufacturing process for industry, due to its low cost and good formability [14]. This reprocessing route has been previously investigated by Cousins et al. [15], who concluded that such process is feasible for repurposing glass fibre–reinforced thermoplastics. However, the study suggested that such parts should only be used in noncritical applications, such as the construction industry, due to the inferior properties of the recyclate as opposed to the original part [16].

Despite previous attempts, the limitations of thermal reshaping for consolidated industrial waste with thick sections and high-viscosity resins, such as polyether ether ketone (PEEK), remain an open research question. Thermal reshaping is a challenging process since the time of exposure to pressure and temperature induces polymer degradation [17–19]. Furthermore, the applied pressure might induce shear stresses at the interfaces between orthogonal plies, resulting in defects such as wrinkles [20]. Residual stresses may also arise within thermoformed samples, due to the mismatch of the coefficients of thermal expansion of the fibres and the matrix [21,22]. Previous studies in thin laminates (1.8 mm thickness) determined that the most important variable which determines the quality of the final product is the temperature of the mould and the sample prior to pressing [23]. Samples must reach a uniform temperature before being pressed, as temperature variance leads to uneven load distribution during pressing [24], thus impacting sample quality and material properties. Furthermore, energy requirements increase when dealing with thicker samples or more complex geometries, since the heat cycle is longer. Reported thermal reshaping procedures for composites based on polyamide, polypropylene or PEEK matrices target temperatures near or above the melting point, such that the resin's viscosity is reduced, allowing it to flow through the fibres, minimising the number of defects such as voids [25,26]; however, this comes at a very high energy input and cost. Reducing the processing temperature is challenging due to the significant increase in viscosity. Experimental results demonstrate that better mechanical performance is achieved with higher-viscosity PEEK grades processed at high temperatures [27]. In the case of thick samples, differences in local viscosity are also expected due to shear stress gradients along the through-thickness direction during pressing [28], which may result in heterogeneous void distribution. The future development of a low-cost, tool-free, low-carbon, sustainable remoulding procedure relies on systematic characterisation studies on processing parameters, that can minimise the energy input while preserving the excellent mechanical properties of thermoplastic resins, particularly critical for high-value resins such as PEEK.

This project aims to develop a low-cost thermal reshaping method compatible with thick industrial high-value waste to support the transition to a more sustainable circular economy and decrease the amount of recyclable material ending up in landfills. The case study employs offcuts of carbon fibre (CF)/PEEK pipes manufactured for the oil and gas industry. To achieve this, a coupled numerical and experimental methodology is proposed. The analysis aims to evaluate the capability and limitations of the methodology by studying the influence of various geometries (e.g., different arc lengths) and processing temperatures on the reduction in curvature of the samples. X-ray computed microtomography (Micro CT) inspection methods are employed to assess the resulting quality in terms of void content. Final guidelines to remould the waste pipes for different applications at a minimum energy cost are provided.

2. Materials and methods

2.1. Sample preparation

The samples to be remoulded were cylindrical CF/PEEK pipes manufactured using laser tape placement provided by Magma Global. They had no prior exposure to hydrocarbon products or the marine environment. They were manufactured from high fibre volume carbon fibre unidirectional PEEK tapes. These tapes were fused by laser, layer by layer, onto a PEEK cylindrical liner that acted as the permeability barrier, in a fully automated robotic process [29]. This formed a fully bonded component with a helical microstructure that followed a $\pm\ \theta$ wind angle. The pipe, therefore, comprised two materials with different mechanical properties: the thermoplastic liner and the high-performance structural composite, with a diameter-to-thickness ratio, D/t, of 7,15. A schematic of the dimensions is in Fig. 1(a).

To remould the pipe, it was first cut into arced sections, then heated and pressed to flatten. The pipe was cut using a bandsaw, into multiple sections with arc angles, α, of 25°, 35° and 45°; see Fig. 1(b). Choosing an arc angle less than 25° would lead to a smaller recyclate, thus its use once thermoformed would be limited to smaller parts. For arc angles greater than 45°, pressing becomes more complex as the normal reaction forces could lead to local compressive failure due to fibre kinking.

2.2. Remoulding

To thermoform the samples, a 130 ton RTM/SQRTM Press by Radius Engineering was used, which allows independently regulating the temperature-pressure cycle. The samples were initially aligned between two hot plates and placed within the press, as in Fig. 2(a). The samples were wrapped in Teflon foil to control spillage of the resin during pressing. No tooling or additional moulds were employed to explore the limitations of tool-free manufacturing practices, which adhere to sustainability policies and our low-cost target [30]. Fig. 2(b) shows an example of the targeted temperature-pressure cycle used to reshape the samples. On a first step, the temperature of both the top and bottom plates of the press was ramped up from room temperature to 200 °C at a rate of 5 °C/min. This temperature was above the glass transition temperature of the material (143 °C) but well below the melting point (343 °C), providing a significant reduction in energy, which is desirable for sustainable manufacturing. It was selected based on preliminary numerical predictions, analysed in detail in Section 4.2. While the plates were heated, a pressure of 1.4 kPa was introduced to the plates. This magnitude was sufficient to enforce contact between the press and the component, thus heat transfer was initiated through conduction, without introducing significant deformation to the sample. Once the temperature of the plates reached 200 °C, the temperature and pressure were kept constant at 200 °C and 1.4 kPa, respectively, for 20 min to allow sufficient time for the heat transfer process, (see Appendix A). During the second step, the pressure was applied in 10.4 kPa intervals for 5 min, gradually increasing to the maximum pressure value allowed

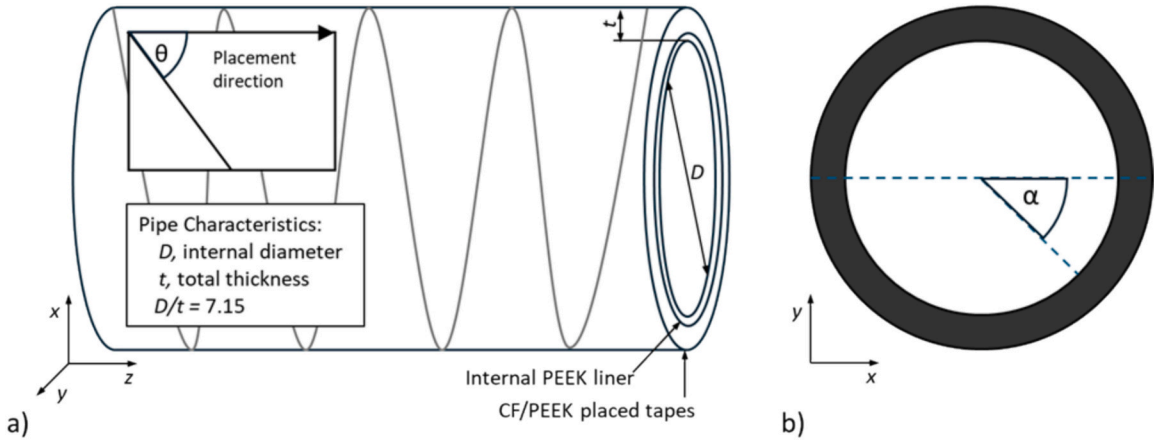

Fig. 1. (a) Schematic view of the pipe characteristics, indicating wind angle, θ, diameter, D, thickness, t, and D/t ratio of 7,15. (b) Cutting procedure with α varying to 25°, 35° and 45° arc angles.

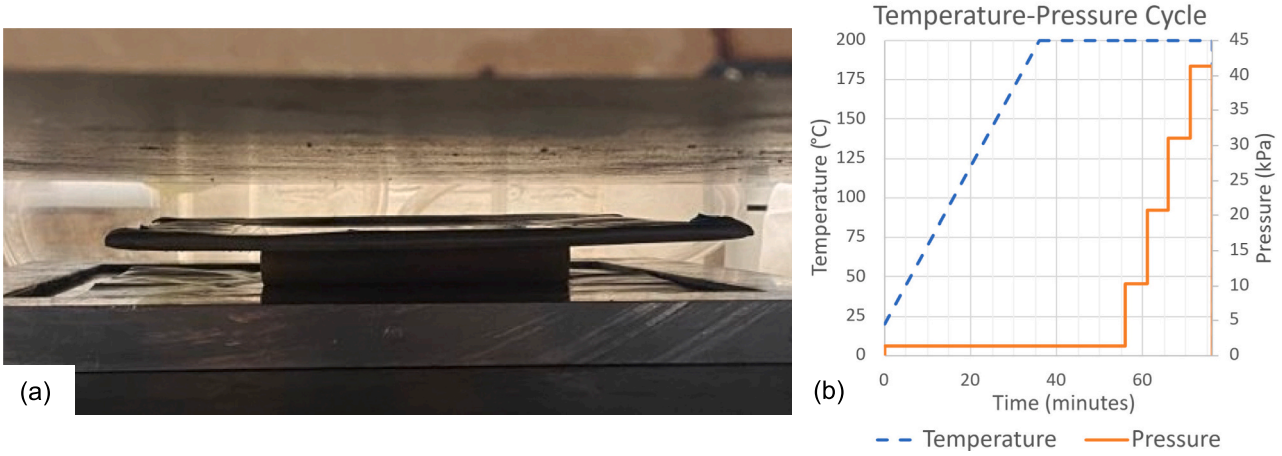

Fig. 2. (a) Sample aligned between the heated plates. (b) Representative temperature-pressure cycle.

by the manufacturing setup. This meant the smallest component (25° arc angle) was subjected to a maximum pressure of 27.5 kPa, while the largest components (35° and 45° arc angle) were subjected to a maximum pressure of 41.4 kPa. The press automatically aborted the operations beyond that point due to unbalanced moments in the press plates resulting from component misalignment. This prevented excessive rotation of the plates, thus avoiding damage to the equipment. The cycle was then terminated, and the sample was removed from the press and left to cool down. No perceptible springback was observed in the samples due to the predominance of plastic deformation mechanisms, the low cooling rate and the relatively low temperatures and pressures applied. Finally, vernier callipers were used to measure the dimensions of the reshaped sample.

Flatness of the sample was evaluated using the geometrical parameter y, as shown in Fig. 3(a), to assess the performance of the thermoforming process for various arc lengths. This parameter indicated a reduction in curvature, so $y = 0$ mm represents a completely flat shape. To measure the initial y for each sample, the outer chord length, C_O, was first measured. Using Fig. 3 (a) and (b), a right-angle triangle was constructed, where $\alpha/2$ was calculated using trigonometric ratios:

$$\sin\left(\frac{\alpha}{2}\right) = \frac{\frac{C_O}{2}}{r+t} \therefore \frac{\alpha}{2} = \arcsin\left(\frac{\frac{C_O}{2}}{r+t}\right) \tag{1}$$

Values for C_O were measured as shown in Fig. 4(a) at three equidistant locations along the depth of each sample, while the pipe's radius, r, was measured prior to cutting the pipe at 76.00 mm. Three measurements of t were also taken for each sample, one at each corner of the profile and one in the centre. Therefore, by plugging r and the mean values of t and C_O in Eq. 1, $\alpha/2$ is calculated. By using trigonometric ratios on the triangle of Fig. 3(a) z, and thus y, can be calculated:

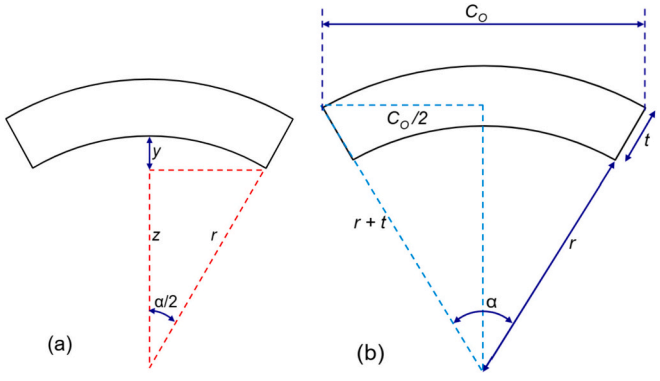

Fig. 3. (a) and (b) Schematics used to calculate the values of y.

$$\cos\left(\frac{\alpha}{2}\right) = \frac{z}{r} \therefore z = r\cos\left(\frac{\alpha}{2}\right) \tag{2}$$

$$y = r - z \tag{3}$$

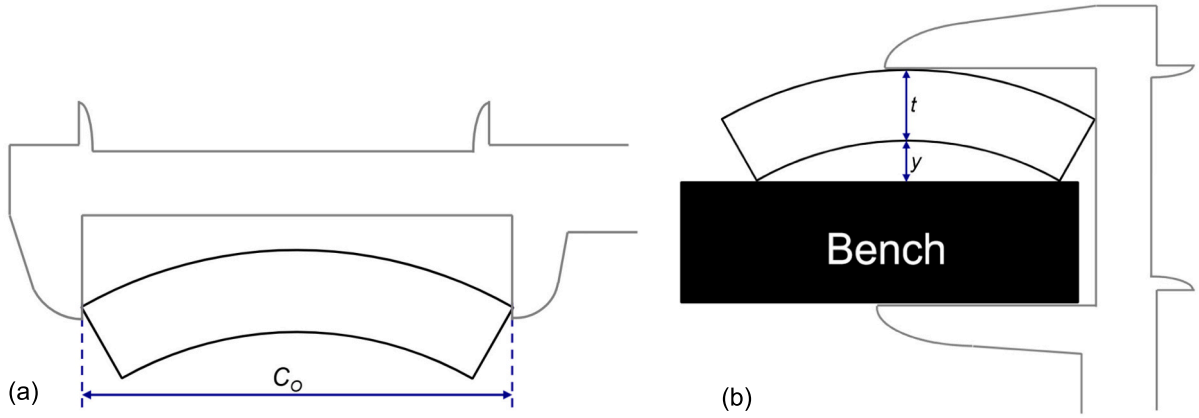

Fig. 4. Measurement procedure of (a) outer chord length, C_o (b) y values of undeformed and thermoformed samples.

The y values of the thermoformed samples were measured using Vernier callipers on a flat bench. The post-thermoformed y value was calculated as the total distance from the bottom of the bench to the top of the sample, minus the thicknesses of the bench and the sample, as shown in Fig. 4(b). To minimise experimental error, due to potential inconsistencies in the thickness of the bench, the vernier calliper was kept at a fixed location, while shifting the samples horizontally.

2.3. Micro CT inspection

Microfocus X-ray computed tomography (Micro CT) scans were performed using a diondo d5® system with a 300 kVp transmission source and a tungsten target. The source was set to 160 kV and 35.2 W (220 μA). Each scan encompassed the recording of 4500 projections during the full 360° rotation of the sample on the tomography stage. Two frames were averaged during the acquisition of each projection, with a 0.28 s exposure time per frame. A 3000 × 3000 pixel VAREX 4343HE flat panel detector was used to record the projection images. The source-to-detector distance was kept at 600 mm, while the source-to-object distance was adjusted for each sample geometry to ensure coverage of the sample width within the scan. Thus, in each case, the reconstructed voxel size was 0.019, 0.021 and 0.027 mm for geometries of arc angles 25°, 35° and 45°, respectively. Image reconstruction was conducted in diondo proprietary software using the Siemens CERA 6.1® engine.

Eleven samples were scanned: nine remoulded specimens (three 25° and 45° arc angle, and two 35° arc angle specimens), and three 'as-received' (untreated) specimens (one of each arc geometry). Post-processing of the reconstructed volumes and estimation of the void content were conducted through Fiji-ImageJ [31,32]. Postprocessing consisted, first, of the application of an unsharp mask filter with a sigma value of 1 and a mask weight of 0.60. A global thresholding method was then used to classify image voxels (3D pixels) into voids (background) and polymer composite (foreground) categories. A cut-off bin index (threshold value) of 100 was chosen to separate both material phases. The separated voids and total sample area were then used to calculate the void fraction.

3. Numerical modelling methodology

Numerical simulations were conducted to investigate the influence of the applied temperature on the stress distribution during remoulding. The simulations were carried out using a finite element model (FEM) implemented in the commercial software Abaqus/Implicit with a coupled temperature-displacement solver.

The FEM visualised in Fig. 5(a) comprises of: (i) two flat rectangular stainless steel plates, representing the press, and (ii) an arced section of 20 mm thickness, representing the sample which is to be reshaped. To reduce the computational cost of the simulations, the sample is discretised by five layers: the inner PEEK liner, and four CF/PEEK of different preferential orientations. This was considered the minimum ply number to capture the effect of interlaminar shear stresses. Layers 1 and 3 have a $+\theta°$ fibre rotation about the longitudinal axis, whereas layers 2 and 4 have a $-\theta°$ fibre rotation, respectively. The sample was discretised using 8-node thermally coupled full-integration solid elements, C3D8T. A structured mesh was used, maintaining the same element size for all geometries, approximately 2 mm in length. The mesh sensitivity study and convergence analysis are available in Appendix B.

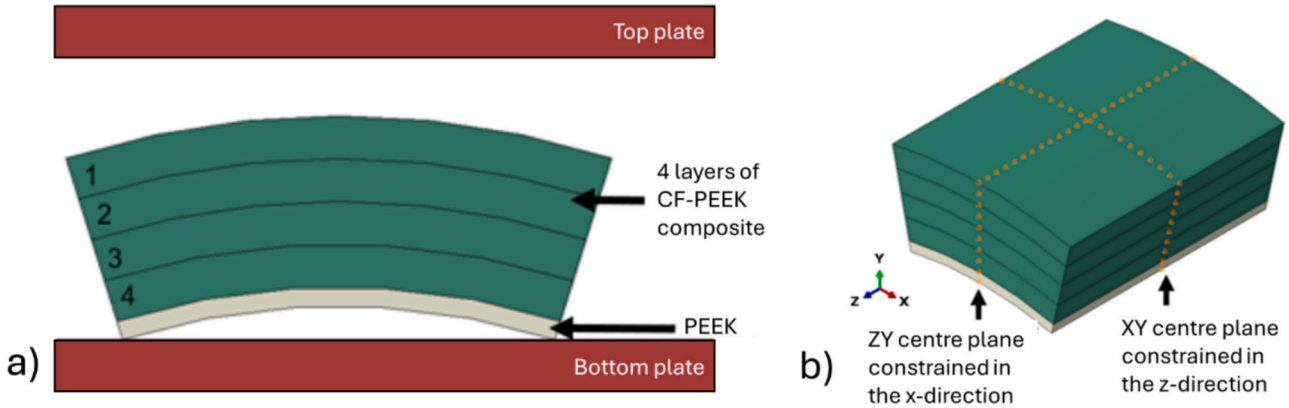

Fig. 5. (a) FEM used to predict the remoulding process numerically. (b) Constraints of the sample.

Different boundary conditions were applied to each part. The bottom mould was fully constrained, as it was assumed to be fixed during remoulding. This was also the case for the top mould, except for vertical displacement (Y direction), thus the top mould is free to move vertically. For the sample, the nodes lying on the ZY centre plane are constrained in the X-direction, whereas the nodes lying in the XY centre plane are constrained in the *Z*-direction, as in Fig. 5(b).

A coupled temperature-displacement step, accounting for a transient thermomechanical response, was defined with a total pseudo-period of 10 s. The top mould was also assigned a velocity of 1 mm/s in the negative Y direction, with a total final displacement of 10 mm. The final gap, therefore, between the top and bottom mould, is equal to the thickness of the sample, 20 mm. Frictionless contact between the sample and the mould is then defined in both tangential and normal directions.

The stainless steel press plates were defined as an isotropic linear elastic material with constant properties for the temperature ranges selected. This included the material's Young's modulus, E, Poisson's ratio, ν, density, ρ, thermal conductivity, k, and specific heat capacity, c, values obtained through Granta [33] for stainless steel. See properties in Table 1.

The PEEK inner liner was defined as an isotropic linear elastic material. Its physical properties (density, thermal conductivity and specific heat capacity) were assumed constant for the chosen temperature range and are available in Table 2. Its Young's modulus was assumed to progressively decrease with temperature, according to Fig. 6(a). For temperatures of up to 150 °C, data were obtained through Granta [33], whereas for higher temperatures, data were obtained from the literature, extrapolating stiffness measurements at room temperature with previous results on the storage modulus characterised by dynamic mechanical analysis [34]. The Poisson's ratio, ν_{12}, is considered constant and equal to 0.40 due to the difficulties of obtaining convergence of incompressible samples with the current solver.

The CF/PEEK tape was defined as orthotropic linear elastic. Its physical properties were also considered constant during thermoforming, see Table 2. The longitudinal Young's modulus was considered constant with a value of 164,84 GPa since this property is predominantly driven by the carbon fibres, and negligible degradation was expected within the temperature range selected [24]. The perpendicular Young's modulus, E_2, is assumed to degrade with the temperature, according to Fig. 6(b). For temperatures lower than 120 °C, values were obtained through literature [24]. For higher temperatures, data were obtained from previously reported Dynamic Mechanical Analysis measurements [34], scaled accordingly to account for differences between the storage modulus, a dynamic measurement that depends on frequency, and quasi-static stiffness, the slope of the stress-strain constitutive curves. Similar degradation rates have been implemented for all the shear stiffnesses. The Poisson's ratios, ν_{12} and ν_{23}, are assumed to remain constant at 0.35 and 0.48, respectively. The thermal conductivity includes a linear dependence with temperature, and has been extrapolated from previous reported experimental values [35].

4. Results

4.1. Thermal reshaping

Fig. 7(a) shows representative remoulded samples with different arc angles compared to the undeformed theoretical circular outlines. Mean measured y values pre- and post-remoulding (Eq. 2), with their standard deviations, and the resulting percentage decrease in y as a measurement of performance of thermal reshaping are in Fig. 7(b). No cracks between adjacent CF tapes were visually observed. A higher flow of the inner PEEK liner compared to the reinforced tape was exhibited. However, the adhesion between both materials remained strong. Despite the relatively low temperature of the process, well below the melting point of PEEK, an increment in flatness is observed in all cases, which is a significant finding considering the high viscosity of the system. A physical limitation in y of approximately 1 mm is found for the applied pressure of 27.5 kPa and processing temperature of 200 °C. The reshaping process was quite repeatable, showing a low scattering in final geometries, mostly associated with the initial hand cutting of the samples, resulting in pre- and post-remoulding y measurements with very similar scattering.

The results of Fig. 7 suggest thermal reshaping is more effective as the arc angle increases, achieving higher flattening rates. This is reasonable since samples with a larger arc angle have more room to displace vertically downwards. On average, a percentage decrease of 32%, 60%, and 65% was achieved in y when remoulding samples with arc angles of 25°, 35°, and 45°, respectively. The lower performance exhibited for arc angles of 25° is also associated with the lower pressure applied (27.5 kPa vs 41.4 kPa), which shows the experimental difficulties in reshaping these components without additional moulds or tooling. Since the absolute y values of 35° thermoformed samples are very close to those of 25° while being nearly half those of 45° samples, 35° is deemed the most optimal reshaping arc angle.

Fig. 8 compares the experimental and numerical results for the final deformation, and the predicted and measured deformed outer chord lengths are shown in Table 3. The finite element model predicted global deformation with high accuracy, with a maximum relative error of 3.51% for the 25° arc length specimen, and predictions within the experimental scatter for the 25° and 45° arc length configurations. The overestimation of the outer chord length was probably due to uncertainty in material properties at temperatures above the glass transition temperature, particularly the stiffness of the carbon fibre tapes in the perpendicular direction.

Fig. 3 shows the predicted deformation contour plots for the corresponding experimental flattening levels. The strain components associated with the matrix cracking failure mode (in-plane 22 and out-of-plane 33) are shown through a cut on the central ZY plane, as indicated in Fig. 5(b). Negligible deformations are present in the 25° sample, in agreement with the lowest percentage reduction in y and experimental applied pressure (27.5 kPa). The deformation tends to increase progressively with the arc angle, exhibiting higher strain levels in the in-plane than in the out-of-plane directions. Two distinct regions are present, split by the neutral axis of the component, in agreement with the analytical theory and experimental observations in nonlinear curved beams [36]. Below the neutral axis, the component exhibits large tensile deformation along the in-plane direction (22) but compressive out-of-plane deformation (33). On the other hand, above the neutral axis, the component undergoes compressive in-plane deformation (22), but experiences tensile out-of-plane deformation (33), with a noticeable edge effect that leads to a significant strain gradient.

Damage accumulation and defects on the remoulded samples were

Table 1
Mechanical and thermal properties of the stainless steel plates [33].

Property	Value
Density, ρ (kg/m^3)	7850
Young's modulus, E (GPa)	210
Poisson's ratio, ν	0.30
Thermal conductivity, k (W/mK)	25
Specific heat capacity, c (J/kg°C)	500

Table 2
Density, ρ, thermal conductivity, k, and specific heat capacity, c, for both PEEK and CF/PEEK [33,35].

Physical properties	CF/PEEK composite	PEEK inner liner
Density, ρ (kg/m^3)	1430	1310
Thermal conductivity, k (W/mK)	5.3 (at 20 °C) [ref 31] 8.9 (at 130 °C) [ref 35] 12.6 (at 240 °C) [ref 35]	0.25
Specific heat capacity, c (J/kgK)	950	1340

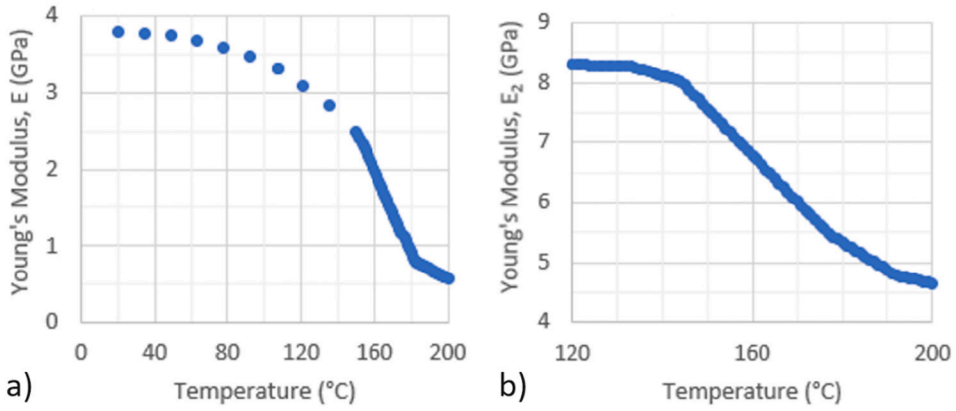

Fig. 6. Stiffness against temperature graphs for (a) PEEK Young's modulus and (b) CF/PEEK Young's modulus along material direction 22.

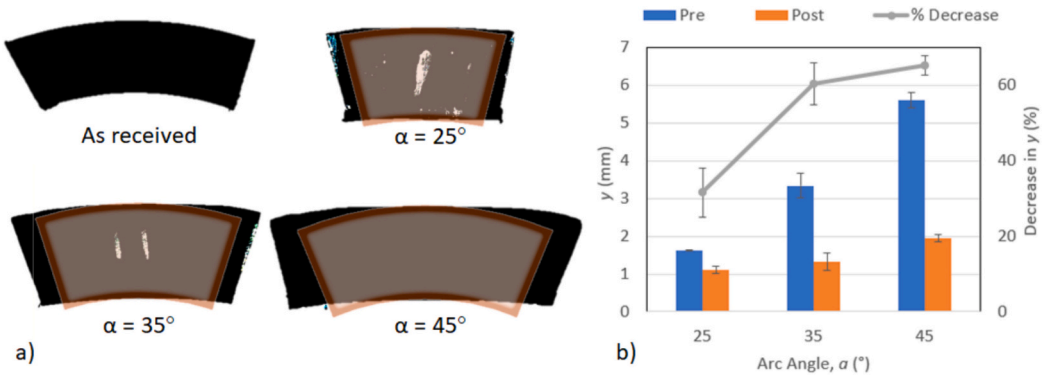

Fig. 7. (a) Representative outlines of remoulded samples in black, and comparison with the undeformed theoretical circular profile in orange. (b) Graph of pre- and post-remoulding y values and the percentage decrease of the y value.

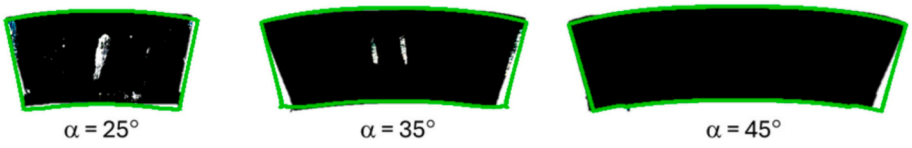

Fig. 8. Comparison between experimental and numerical results in terms of overall deformation for 25°, 35° and 45° arc angles. Experimental images are shown in black, and predicted FEM profiles are shown in light green. (For interpretation of the references to colour in this figure legend, the reader is referred to the web version of this article.)

Table 3
Comparison between experimental and numerical deformed outer chord length, C_O of thermally reshaped samples, measured as per Fig. 4(a).

Method/Arc angle	Numerical [mm]	Experimental [mm]	Relative error [%]
25°	41.44	40.04 ± 1.18	3.51
35°	57.24	55.40 ± 1.26	3.32
45°	72.73	71.80 ± 1.91	1.29

investigated by X-ray micro CT. The samples exhibit the characteristic microstructure of laser tape placement composites, with morphological features similar to those previously reported in the literature [37–39]. Fig. 10 plots the normalised void fraction by the mean void volume of the as-received samples. Overall, thermal reshaping increases porosity and scattering, resulting in tape deconsolidation. Deconsolidation is a conventional failure mode of laser-assisted automated fibre placement thermoplastic composites, which promotes interlaminar delamination and tape debonding [40,41]. It occurs when the residual stresses stored in the tapes are released upon reheating beyond the glass transition temperature. In our study, the release of stress occurs during the warming stage before applying pressure with the press, see Fig. 2(b). Other defects associated with fibre placement, such as fibre waviness or wrinkling [29], are not observed, as the thermal reshaped samples maintain the original fibre alignment.

The samples with arc angles of 45° present the lowest void content compared to the 25° and 35° counterparts, as shown in Fig. 10. Further analysis of the results as a function of the stress state is conducted by dividing the specimens into two regions: below and above the neutral axis, undergoing in-plane tensile or compressive deformation, respectively, as predicted by FEM. A beneficial effect of large in-plane compressive deformation ($\varepsilon_{22} < 0$) is observed, with a significant reduction in mean void content and scattering. Furthermore, compression on the through-thickness direction ($\varepsilon_{33} < 0$) might also contribute to reducing the void content in the regions submitted to in-plane tension. However, a higher number of inspected samples is needed for robust confirmation. This reduction of void content was not registered in components with smaller arc angles, demonstrating that minimum consolidation stresses are necessary during remoulding to reduce defects produced by deconsolidation and achieve reliable quality. These

findings align with prior research, where increased consolidation pressures led to a reduction in void content and improved mechanical properties [42,43].

4.2. Numerical predictions of the influence of processing parameters

This section numerically explores the feasibility of low-cost thermal reshaping for increased processing pressures and temperatures using the finite element model described in Section 3. The feasibility studies consider the fibre's strength as the primary physical limitation. The first parametric numerical study compares the experimental stresses along the fibre direction to the fibre's strength as a function of the progressive flattening. This is shown in Fig. 11, where the relations of calculated longitudinal tensile and compressive stresses at the bottom and top surfaces of the samples are plotted against sample decrement in y (%), at a processing temperature of 200 °C. The black circles indicate the predicted longitudinal stresses at the measured y (%) decrement after the experimental procedure. The straight line represents the longitudinal compressive strength material property of a comparable CF/PEEK unidirectional composite previously reported in the literature [26], used to compare with the longitudinal compressive stress predicted at the finite-element integration points.

As expected, longitudinal stress increases as y decreases, given that more pressure is applied to the samples to induce further flattening. Stresses induced within the 35° and 45° samples are sufficiently higher than those of the 25° ones, potentially exceeding the CF's compressive strength at very high y (%) decrements. This suggests that thermoforming might have limitations when processing large samples at high pressures and low temperatures, resulting in failure due to high compressive stresses and fibre kinking, and posing considerable difficulties in processing samples with arc angles greater than 45°.

The second parametric numerical study explores the change in longitudinal stresses of each sample size as processing temperature increases while Y decrement is set to 100% (perfectly flat samples). The results are plotted in Fig. 12, where both calculated tensile and compressive longitudinal stresses are recorded at the bottom and top surfaces of the pipe respectively, from 120 °C until 240 °C at an increment set to 20 °C.

The evolution of the predicted stresses with increasing temperature follows the curvature of the material's mechanical properties, as indicated in Fig. 6. This is reasonable given that the samples' response is highly dependent on their mechanical properties, which are dictated by the processing temperature. The findings indicate that all sample sizes would fail due to compression if fully flattened at processing temperatures below 160 °C. For processing temperatures of 180 °C–200 °C, processing the 25° samples becomes feasible, with stress values below the material's compressive strength. Meanwhile, the stresses in 35° and 45° samples are still higher than the material's compressive strength. For temperatures higher than 220 °C, all sample sizes present stresses lower than the fibre's compressive strength, even though such stresses for the 35° and 45° samples are borderline.

5. Discussion

Low-cost remoulding yields varied performance when reshaping thick semicircular components of different sizes. The baseline processing parameters (200 °C of temperature and a maximum pressure of 41.4 kPa) result in a trade-off between the absolute flatness and void content of the new part. For instance, if absolute flatness is the critical requirement, then smaller arc angles (e.g., 25°) should be used. This can be seen in Fig. 7, where the lowest absolute y is that of 25°, even though the applied pressure was 27.5 kPa, compared to 41.4 kPa applied for the larger samples. Fig. 11 also suggests this, where compressive stresses at 100% Y decrement are sufficiently lower than those induced on larger samples. However, this leads to a higher void volume, as a minimum confinement pressure is required to address the debonding caused by deconsolidation, see Fig. 10.

The final produced part consists of a slender rod, assimilating to pultruded and braided composite beams [44,45]. Potential applications include frames in automotive [46], railway [47], aerospace [48], and civil [49] sectors. The main limitation envisaged is the lack of versatility of the original tapes lay-up and orientation. Future investigations should focus on realigning the tapes towards a preferential direction to enhance axial stiffness. This can potentially be achieved by applying in-plane tensile loads during thermal reshaping, extending techniques previously employed for carbon fibre/epoxy composites [50] and needle-punched nonwovens [51].

If flatness is not critical, samples with a larger arc angle can be used to manufacture larger parts. At the expense of higher energy consumption, the compressive stresses generated during the remoulding of large components allow the resin to flow and fill voids and gaps between adjacent tapes, potentially minimising the defects generated during deconsolidation. Reshaped parts could potentially be employed for primary structural applications, recovering the original economic value of the virgin material. This could be achieved by splitting and sectioning into strips to create new stacking sequences, as suggested by Cousins et al. [15].

These findings emphasise the successful application of thermal reshaping to repurpose high-value thick composite sections based on high-viscosity resins such as PEEK. This method was previously limited to short-fibre composite products [52], thin sheets [23,53,54], or low-viscosity thermoplastic systems such as Elium [15]. Furthermore, the proposed reshaping technique, with a short heating cycle of 80 min for a 20 mm thickness component, should minimise thermal resin degradation compared to the 8 h cycle previously used, preserving the original mechanical properties [15,17]. Nevertheless, additional factors should be considered to extend the method for repurposing decommissioned PEEK composite pipes, given their long exposure to the marine environment. Despite the low reactivity [55] and good chemical stability [56] of semi-crystalline PEEK at low temperatures, saturated samples may exhibit differences in thermal and mechanical responses, with expected changes in their glass transition temperature [57] and a gradual degradation of mechanical properties whilst in its saturated state [58]. Drying the PEEK composite should enable the sample to be reprocessed above the melting temperatures. However, the capabilities of low-cost thermal reshaping applied to decommissioned pipes need to be experimentally assessed in future studies. To maximise the economic value of the recovered material, additional testing is required to assess sample quality and mechanical performance and determine their suitability for structural applications.

Another important aspect to examine is how the ratio of the PEEK liner thickness to the CF/PEEK layer affects thermal reshaping. Considering the pipe's bending response during this process, a thicker liner would prevent compressive failure of the bottom layers, enabling processing at lower temperatures. However, the influence of liner thickness on through-thickness compression stresses is complex, as multiple mechanisms must be considered separately. For instance, a thicker liner may promote resin flow, but at the same time, decrease through-thickness compression (see Fig. 9 d, e, and f), which is necessary to minimise porosity in the carbon fibre tape layers.

However, low-cost thermal reshaping does not come without practical and physical limitations. The practical limitation of our study involves applying even pressure to the component without using additional moulds. As a result of misalignments, bending moments are imposed in the heated plates, aborting the moulding operations at relatively low-pressure levels. The addition of a steel mould that ensures the position of the component within the press should alleviate this issue, allowing the application of higher pressures and, therefore, obtaining higher flattening levels. However, the additional cost of the mould, the thermal energy needed to heat it, and additional manufacturing operations such as part demoulding and mould maintenance should be considered in life cycle assessments.

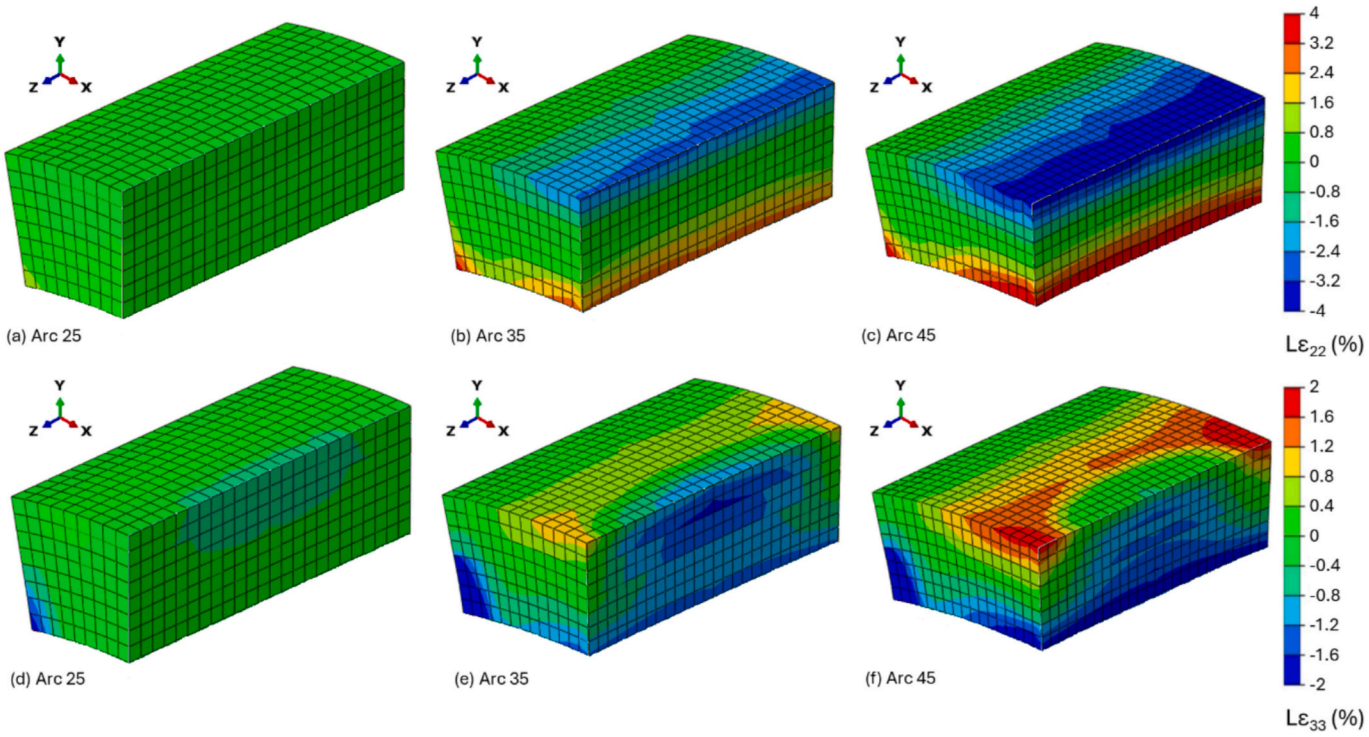

Fig. 9. Predicted strain fields of the CF tapes along material direction 22 for the arc angles (a) $\alpha = 25°$, (b) $\alpha = 35°$, and (c) $\alpha = 45°$ and material direction 33 for (d) $\alpha = 25°$, (e) $\alpha = 35°$, and (f) $\alpha = 45°$.

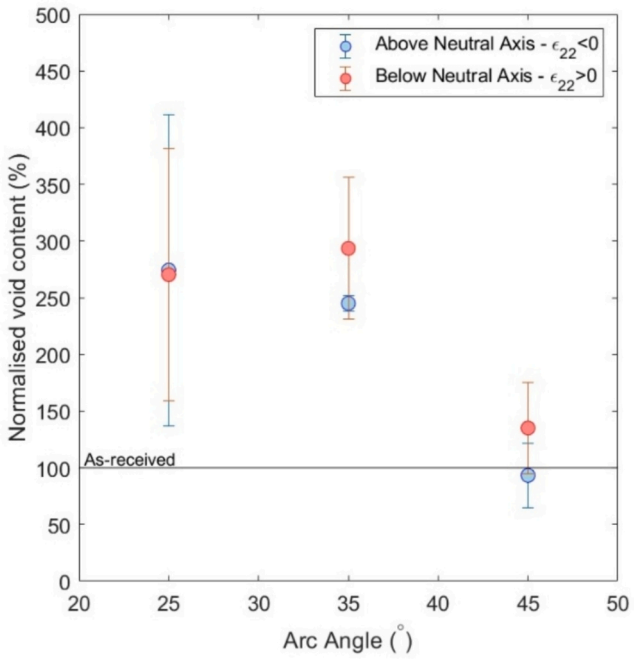

Fig. 10. Normalised void content after thermal reshaping as a function of the arc length. Comparison between regions below and above the neutral axis, subjected to in-plane tensile or compressive deformation, ε_{22}.

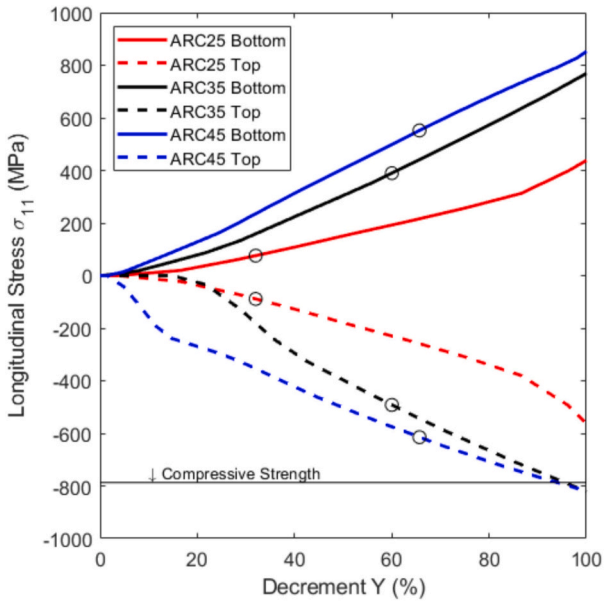

Fig. 11. Calculated maximum longitudinal fibre stresses for increased pressures (and increased flattening) for a processing temperature of 200 °C. Compressive strength value obtained from the literature [26].

A customised mould could also offer additional benefits for thermal reshaping, especially when using hybrid moulds [59]. Hybrid moulds, equipped with multiple compliance inserts, can accurately control the applied confinement pressure to ensure the quality of the part, ultimately minimising the void content. This will allow for the maximisation of the sample's flatness and quality, eliminating the need for a trade-off. This provides a viable alternative to conventional tension springs in reverse forming, which can lead to matrix cracking, wrinkles, and tape misalignment due to the imposed tensile stresses [25]. Lastly, a hybrid mould could allow for the creation of more complex final geometries, such as corrugated panels [60] or vehicle body parts [61].

Despite the previous, even hybrid moulds may not be able to completely flatten the largest components due to the physical limitations imposed by the compressive strength of the CF/PEEK tape. While

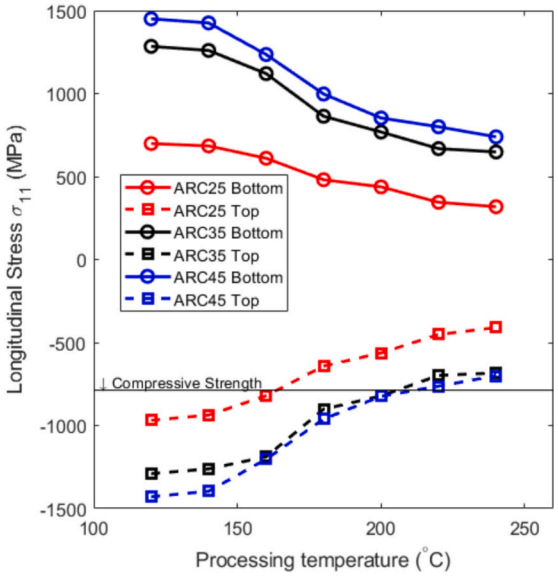

Fig. 12. Calculated maximum longitudinal fibre stresses as a function of the processing temperature for full component flattened (*y* decrement of 100%).

increasing the compressive stresses perpendicular to the fibre direction has been found to improve the component's quality, our numerical results indicate that large components will be vulnerable to compressive fibre failure at high levels of flattening, even at increased temperatures, see Fig. 12. It is essential to achieve a balance between compressive longitudinal and transverse stresses so that the confinement pressure is high enough to allow the resin to flow and reduce void content without causing compressive failure on the top surface of the pipes. In our study, the results suggest that full flattening can be achieved for 25° samples at a processing temperature above 180 °C, whereas 35° and 45° samples can only be fully flattened at temperatures higher than 220 °C. However, the predicted compressive stresses are still very close to the material's compressive strength, so this assumption should be verified experimentally. Future work should analyse failure in detail during thermal reshaping, including the development of physically based temperature-dependent failure criteria that account for the composite's deformation and failure mechanisms above the glass transition temperature.

6. Conclusions

A low-cost sustainable thermal reshaping process for thick industrial composite waste has been studied from an experimental and numerical point of view. It employed industrial carbon-fibre PEEK waste pipes from the oil and gas industry as a case study, a high-value and high-performance fibre/resin system, currently disposed of as landfill.

The experimental procedure led to a 65% reduction in curvature of the semicircular sections, despite the high viscosity of the PEEK resin, at relatively low pressures and temperatures applied, which were well below the melting point. Micro-CT inspection revealed a beneficial impact of the confinement pressure, reducing the local void content in regions subjected to compressive transverse stresses. This relatively low-energy processing procedure resulted in repeatable and reproducible final geometries of the reshaped samples, showing the potential of tool-free remoulding to reshape thick composite waste. It also offers an alternative to reshaping and recycling methods that fully melt the resin, preserving the chemical and mechanical properties of the high-value PEEK resin.

The numerical parametric studies provided additional guidelines for thermal reshaping. The numerical results showed limitations to reshaping specimens with large arc lengths (e.g., 35° and 45°) due to the development of high compressive stresses along the fibre direction, even at elevated temperatures. The simulations also demonstrated the potential to reduce the processing temperature further to flatten smaller samples with arc lengths 25° from 200 to 180 °C if larger pressures are applied.

All three arc angles tested could be used in different applications; smaller arc angles can be reshaped in parts where flatness is critical, while larger arc angles can be reshaped into larger-sized parts. Future studies should focus on the influence of processing temperatures and pressure on the degradation of chemical, thermal and mechanical properties, and the ability to obtain additional complex shapes for 3-D composite parts with minimal residual stresses.

CRediT authorship contribution statement

Antreas Potsis: Writing – original draft, Validation, Software, Resources, Methodology, Investigation, Formal analysis, Data curation. **Fernando Álvarez-Borges:** Writing – review & editing, Methodology, Investigation, Data curation. **Irene Jiménez-Fortunato:** Writing – review & editing, Methodology, Funding acquisition. **Erick Montes de Oca Valle:** Writing – review & editing, Methodology, Funding acquisition. **Francisca Martínez-Hergueta:** Writing – original draft, Visualization, Validation, Supervision, Project administration, Methodology, Investigation, Funding acquisition, Formal analysis, Conceptualization.

Declaration of competing interest

The authors declare that they have no known competing financial interests or personal relationships that could have appeared to influence the work reported in this paper.

Acknowledgements

The authors would like to acknowledge the support of the School of Engineering of The University of Edinburgh to conduct this research. Non-destructive inspection was carried out at the μ-VIS X-ray Imaging Centre, University of Southampton, part of the National Research Facility for Lab-based X-Ray Computed Tomography [grant number EP/T02593X/1]. Dr. Brian Peterson's and Elsa Kapitan-White's comments are greatly appreciated. The authors would also like to thank Magma Global and TechnipFMC for permission to publish this paper.

Appendix A. Numerical modelling of heat transfer

The duration of the heating stage in the thermal reshaping process was estimated using predictions from a finite element model, following the approach in Section 3. A transient heat transfer analysis was set up with a total duration of 15 min and a fixed time step of 30 s, resulting in 30 increments. The pipe was placed in direct contact with the top and bottom mould plates, ensuring no gaps between them. A thermal conductance interaction was assigned for all interacting surfaces in the model, neglecting the effects of thermal convection. The boundary conditions included a fixed temperature of 200 °C for the top and bottom steel plates, while the sample's initial temperature was set to room temperature (20 °C).

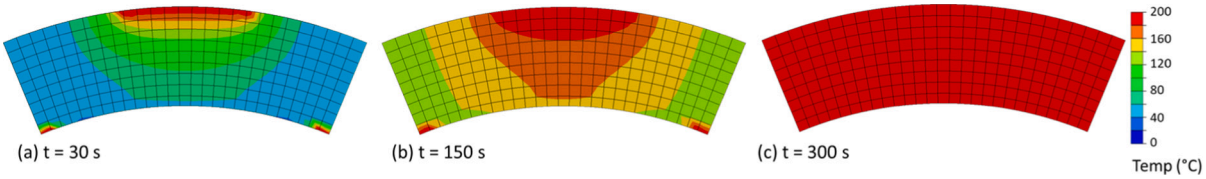

Fig. A1. Predicted evolution of the temperature distribution of the 45° samples during the warming stage. (a) 30 s, (b) 150 s and (c) 300 s.

Fig. A1 shows the predicted evolution of the temperature distribution when heating a sample with an arc length of 45°. It shows that a constant temperature of 200 °C is reached after 300 s. Since this sample represents the largest volume of material tested, it is assumed that smaller samples with arc lengths of 25° and 35° will heat up more quickly. Based on these results, a holding time of 20 min was chosen as a conservative value to ensure the samples reach a stable temperature before the pressure is applied and reshaping is initiated.

Appendix B. Numerical model validation and mesh sensitivity analysis

To assess the validity of the numerical modelling study, a mesh convergence analysis was conducted. This was carried out on the sample expected to exhibit the highest stress gradients, the 45° arc configuration at 120 °C. Fig. A2 shows the maximum compressive stress as a function of the number of elements in the pipe component, alongside the computational cost with an Intel Core i5 8th generation 4 core CPU. Convergence is found after a model size of 6000 elements. Considering this, a mesh size of 2 mm, corresponding to 7560 elements, was selected to model the pipes, ensuring accurate predictions with minimal computational cost.

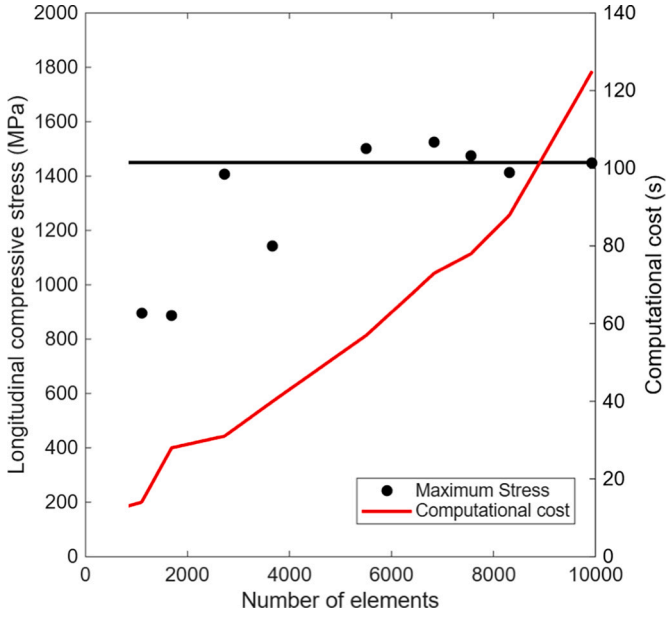

Fig. A2. Mesh convergence plot reporting maximum compressive stresses along the longitudinal fibre directions and computational cost.

References

[1] Chen W, Zhang Q, Cao H, Yuan Y. Process evaluation, tensile properties, mathematical models, and fracture behavior of 3D printed continuous fiber reinforced thermoplastic composites. J Reinforced Plastic Compos 2021;40:845–63. https://doi.org/10.1177/07316844211016091.

[2] Mrazova M. Advanced composite materials of the future in aerospace industry. INCAS BULLETIN 2013;5:139–50. https://doi.org/10.13111/2066-8201.2013.5.3.14.

[3] Yu K, Morozov EV, Ashraf MA, Shankar K. A review of the design and analysis of reinforced thermoplastic pipes for offshore applications. J Reinforced Plastic Compos 2017;36:1514–30. https://doi.org/10.1177/0731684417713666.

[4] Ahmad H, Markina AA, Porotnikov MV, Ahmad F. A review of carbon fiber materials in automotive industry. IOP Confer Series Mater Sci Eng 2020;971:032011. https://doi.org/10.1088/1757-899x/971/3/032011.

[5] Compton BG, Post BK, Duty CE, Love L, Kunc V. Thermal analysis of additive manufacturing of large-scale thermoplastic polymer composites. Addit Manuf 2017;17:77–86. https://doi.org/10.1016/j.addma.2017.07.006.

[6] Shuaib NA, Mativenga PT, Kazie J, Job S. Resource efficiency and composite waste in UK supply chain. Procedia CIRP 2015;29:662–7. https://doi.org/10.1016/j.procir.2015.02.042.

[7] Lenzi D, Jakob M, Honegger M, Droege S, Heyward JC, Kruger T. Equity implications of net zero visions. Clim Change 2021;169. https://doi.org/10.1007/s10584-021-03270-2.

[8] Post W, Susa A, Blaauw R, Molenveld K, Knoop RJI. A review on the potential and limitations of recyclable thermosets for structural applications. Polym Rev 2019;60:359–88. https://doi.org/10.1080/15583724.2019.1673406.

[9] Pegoretti A. Towards sustainable structural composites: a review on the recycling of continuous-fiber-reinforced thermoplastics. Adv Indus Eng Polym Res 2021;4:105–15. https://doi.org/10.1016/j.aiepr.2021.03.001.

[10] Morin C, Loppinet-Serani A, Cansell F, Aymonier C. Near- and supercritical solvolysis of carbon fibre reinforced polymers (CFRPs) for recycling carbon fibers as a valuable resource: state of the art. J Supercrit Fluids 2012;66:232–40. https://doi.org/10.1016/j.supflu.2012.02.001.

[11] Swamy JN, Grouve WJ, Wijskamp S, Akkerman R. An experimental study on the role of different void removal mechanisms in VBO processing of advanced thermoplastic composites. J Reinf Plast Compos 2023;43:183–94. https://doi.org/10.1177/07316844231159134.

[12] Bernatas R, Dagreou S, Despax-Ferreres A, Barasinski A. Recycling of fiber reinforced composites with a focus on thermoplastic composites. Cleaner Eng Technol 2021;5:1–14. https://doi.org/10.1016/j.clet.2021.100272.

[13] Throne JL. Understanding thermoforming. 2nd ed. Munich: Carl Hanser Verlag; 2008.

[14] Yang C, Hung SW. Modeling and optimization of a plastic thermoforming process. J Reinforced Plastic Compos 2004;23:109–21. https://doi.org/10.1177/0731684404029324.
[15] Cousins DS, Suzuki Y, Murray RE, Samaniuk JR, Stebner AP. Recycling glass fiber thermoplastic composites from wind turbine blades. J Clean Prod 2019;209:1252–63. https://doi.org/10.1016/j.jclepro.2018.10.286.
[16] La Mantia FP. Mechanical properties of recycled polymers. Macromolec Symposia 1999;147:167–72. https://doi.org/10.1002/masy.19991470116.
[17] Pascual A, Toma M, Tsotra P, Grob MC. On the stability of PEEK for short processing cycles at high temperatures and oxygen-containing atmosphere. Polym Degrad Stab 2019;165:161–9. https://doi.org/10.1016/j.polymdegradstab.2019.04.025.
[18] McLauchlin AR, Ghita OR, Savage L. Studies on the reprocessability of poly(ether ether ketone) (PEEK). J Mater Process Technol 2014;214:75–80. https://doi.org/10.1016/j.jmatprotec.2013.07.010.
[19] Dandy LO, Oliveux G, Wood J, Jenkins MJ, Leeke GA. Accelerated degradation of Polyetheretherketone (PEEK) composite materials for recycling applications. Polym Degrad Stab 2015;112:52–62. https://doi.org/10.1016/j.polymdegradstab.2014.12.012.
[20] Harrison P, Campbell I, Guliyev E, McLelland B, Gomes R, Curado-Correia N, et al. Induction melt thermoforming of advanced multi-axial thermoplastic composite laminates. J Manuf Process 2020;60:673–83. https://doi.org/10.1016/j.jmapro.2020.10.026.
[21] Parlevliet PP, Bersee HE, Beukers A. Residual stresses in thermoplastic composites—a study of the literature—part I: formation of residual stresses. Compos A: Appl Sci Manuf 2006;37:1847–57. https://doi.org/10.1016/j.compositesa.2005.12.025.
[22] Trende A, Åström BT, Nilsson G. Modelling of residual stresses in compression moulded glass-mat reinforced thermoplastics. Compos A: Appl Sci Manuf 2000;31:1241–54. https://doi.org/10.1016/s1359-835x(00)00078-6.
[23] McCool R, Murphy A, Wilson R, Jiang Z, Price M, Butterfield J, et al. Thermoforming carbon fibre-reinforced thermoplastic composites. Proc Inst Mech Eng L J Mater Des Appl 2012;226:91–102. https://doi.org/10.1177/1464420712437318.
[24] Melo JDD, Radford DW. Viscoelastic properties of PEEK-IM7 related to temperature. J Reinforced Plastic Compos 2005;24:545–56. https://doi.org/10.1177/0731684405045019.
[25] Kiss P, Stadlbauer W, Burgstaller C, Stadler H, Fehringer S, Haeuserer F, et al. In-house recycling of carbon- and glass fibre-reinforced thermoplastic composite laminate waste into high-performance sheet materials. Compos A: Appl Sci Manuf 2020;139:106110. https://doi.org/10.1016/j.compositesa.2020.106110.
[26] Pheysey J, De Cola F, Pellegrino A, Martinez-Hergueta F. Strain rate and temperature dependence of short/unidirectional carbon fibre PEEK hybrid composites. Compos Part B Eng 2024;268:111080. https://doi.org/10.1016/j.compositesb.2023.111080.
[27] Curmi A, Rochman A, Buhagiar J. Influence of polyether ether ketone (PEEK) viscosity on interlayer shear strength in screw extrusion additive manufacturing. Addit Manuf 2024;84:104086. https://doi.org/10.1016/j.addma.2024.104086.
[28] Yan M, Tian X, Peng G, Li D, Zhang X. High temperature rheological behavior and sintering kinetics of CF/PEEK composites during selective laser sintering. Compos Sci Technol 2018;165:140–7. https://doi.org/10.1016/j.compscitech.2018.06.023.
[29] Okolie O, Latto J, Faisal N, Jamieson H, Mukherji A, Njuguna J. Manufacturing defects in thermoplastic composite pipes and their effect on the in-situ performance of thermoplastic composite pipes in oil and gas applications. Appl Compos Mater 2022;30:231–306. https://doi.org/10.1007/s10443-022-10066-9.
[30] Sarfraz MS, Hong H, Kim SS. Recent developments in the manufacturing technologies of composite components and their cost-effectiveness in the automotive industry: a review study. Compos Struct 2021;266:113864. https://doi.org/10.1016/j.compstruct.2021.113864.
[31] Schindelin J, Arganda-Carreras I, Frise E, Kaynig V, Longair M, Pietzsch T, et al. Fiji: an open-source platform for biological-image analysis. Nat Methods 2012;9:676–82. https://doi.org/10.1038/nmeth.2019.
[32] Schneider CA, Rasband WS, Eliceiri KW. NIH image to ImageJ: 25 years of image analysis. Nat Methods 2012;9:671–5. https://doi.org/10.1038/nmeth.2089.
[33] Ansys Inc. PEEK (30% carbon fiber), PEEK and stainless steel. Granta Edupack; 2023. R1 [software].
[34] Papageorgiou DG, Liu M, Li Z, Vallés C, Young RJ, Kinloch IA. Hybrid poly(ether ether ketone) composites reinforced with a combination of carbon fibres and graphene nanoplatelets. Compos Sci Technol 2019;175:60–8. https://doi.org/10.1016/j.compscitech.2019.03.006.
[35] Comelli C, Yi N, Davies R, van der Pol H, Ghita O. Observation of peek melting peaks within the additive manufacturing material extrusion process in relation to isothermal and non-isothermal processes. Macromol Mater Eng 2024;309(4):2300386. https://doi.org/10.1002/mame.202300386.
[36] Falope FO, Lanzoni L, Tarantino AM. The bending of fully nonlinear beams. Theoretical, numerical and experimental analyses. Int J Eng Sci 2019;145:103167. https://doi.org/10.1016/j.ijengsci.2019.103167.
[37] Comer AJ, Ray D, Obande WO, Jones D, Lyons J, Rosca I, et al. Mechanical characterisation of carbon fibre–PEEK manufactured by laser-assisted automated-tape-placement and autoclave. Compos A: Appl Sci Manuf 2015;69:10–20. https://doi.org/10.1016/j.compositesa.2014.10.003.
[38] Dilonardo E, Nacucchi M, De Pascalis F, Zarrelli M, Giannini C. Inspection of carbon fibre reinforced polymers: 3D identification and quantification of components by X-ray CT. Appl Compos Mater 2022;29(2):497–513. https://doi.org/10.1007/s10443-021-09976-x.
[39] Kok R, Cuvillo R, Rodríguez-García V, Pernas J, Artero-Guerrero JA, de Villoria RG, et al. Low velocity impact response of automated fiber placement advanced placed ply composites. Compos Sci Technol 2024;253:110636. https://doi.org/10.1016/j.compscitech.2024.110636.
[40] Fereidouni M, Hoa SV. In-situ consolidation of thermoplastic composites by automated fiber placement: characterization of defects. J Thermoplast Compos Mater 2024;38:471–511. https://doi.org/10.1177/08927057241251837.
[41] Kok R, Martinez-Hergueta F, Teixeira-Dias F. Tensile response of AP-PLY composites: a multiscale experimental and numerical study. Compos A Appl Sci Manufact 2022;159:1–14. https://doi.org/10.1016/j.compositesa.2022.106989.
[42] Saenz-Castillo D, Martín MI, Calvo S, Rodriguez-Lence F, Güemes A. Effect of processing parameters and void content on mechanical properties and NDI of thermoplastic composites. Compos A: Appl Sci Manuf 2019;121:308–20. https://doi.org/10.1016/j.compositesa.2019.03.035.
[43] Ma Y, Zhang Z, Gao T, Pan B, Sun M, Zhang G, et al. Influence of thermal history and consolidation force on wedge peel strength of CF/PEEK laminates manufactured by laser-radiated in-situ consolidation. Polym Compos 2024:1–16. https://doi.org/10.1002/pc.29032.
[44] Bilisik K. Three-dimensional braiding for composites: a review. Textile Res J 2012;83:1414–36. https://doi.org/10.1177/0040517512450766.
[45] Talabi SI, Tobin J, Strom B, Brownstein I, Kunc V, Hassen AA. Recent and future developments in pultrusion technology with consideration for curved geometries: a review. Compos Part B Eng 2024;283:111678. https://doi.org/10.1016/j.compositesb.2024.111678.
[46] Park CK, Kan CD, Hollowell WT. Evaluation of crashworthiness of a carbon-fibre-reinforced polymer (CFRP) ladder frame in a body-on-frame vehicle. Int J Crashworthiness 2013;19:27–41. https://doi.org/10.1080/13588265.2013.830940.
[47] Singh A, Gu Z, Hou X, Liu Y, Hughes DJ. Design optimisation of braided composite beams for lightweight rail structures using machine learning methods. Compos Struct 2022;282:115107. https://doi.org/10.1016/j.compstruct.2021.115107.
[48] Ren Y, Gao B, Liu X, Zheng J. The crashworthiness prediction of 2D triaxially braided composite fuselage frame under transverse impact load. Int J Crashworthiness 2019;25:421–9. https://doi.org/10.1080/13588265.2019.1603850.
[49] Yang X, Bai Y, Ding F. Structural performance of a large-scale space frame assembled using pultruded GFRP composites. Compos Struct 2015;133:986–96. https://doi.org/10.1016/j.compstruct.2015.07.120.
[50] Fuller J, Jalalvand M, Wisnom MR. Combining fibre rotation and fragmentation to achieve pseudo-ductile CFRP laminates. Compos Struct 2016;142:155–66. https://doi.org/10.1016/j.compstruct.2016.01.073.
[51] Martínez-Hergueta F, Ridruejo A, Gálvez F, González C, LLorca J. Influence of fiber orientation on the ballistic performance of needlepunched nonwoven fabrics. Mech Mater 2016;94:106–16. https://doi.org/10.1016/j.mechmat.2015.11.019.
[52] Sun C, Gergely R, Okonski DA, Min J. Experimental and numerical investigations on thermoforming of thermoplastic prepregs of glass fiber reinforced nylon 6. J Mater Process Technol 2021;295:117161. https://doi.org/10.1016/j.jmatprotec.2021.117161.
[53] Chen H, Li S, Wang J, Ding A. A focused review on the thermo-stamping process and simulation progresses of continuous fibre reinforced thermoplastic composites. Compos Part B Eng 2021;224:109196. https://doi.org/10.1016/j.compositesb.2021.109196.
[54] Obande W, Stankovic D, Bajpai A, Devine M, Wurzer C, Lykkeberg A, et al. Thermal reshaping as a route for reuse of end-of-life glass fibre-reinforced acrylic composites. Compos Part B Eng 2023;257:110662. https://doi.org/10.1016/j.compositesb.2023.110662.
[55] Surve K, Krishnamoorti R, Bhowmick A, Chen X. Experimental and simulation studies of the role of water on degradation of polyetheretherketone under high pressure and high temperature conditions. Polym Degrad Stab 2025:111729. https://doi.org/10.1016/j.polymdegradstab.2025.111729.
[56] Kurtz Steven M. Chemical and radiation stability of PEEK. In: PEEK biomaterials handbook. William Andrew Publishing; 2012. p. 75–9. https://doi.org/10.1016/B978-1-4377-4463-7.10006-5.
[57] Boinard E, Pethrick RA, MacFarlane CJ. The influence of thermal history on the dynamic mechanical and dielectric studies of polyetheretherketone exposed to water and brine. Polymer 2000;41(3):1063–76. https://doi.org/10.1016/S0032-3861(99)00259-1.
[58] Liu H, Wang J, Jiang P, Yan F. Accelerated degradation of polyetheretherketone and its composites in the deep sea. R Soc Open Sci 2018;5:171775. https://doi.org/10.1098/rsos.171775.
[59] Martinho PG, Pouzada AS. Alternative materials in moulding elements of hybrid moulds: structural integrity and tribological aspects. Int J Adv Manuf Technol 2021;113:351–63. https://doi.org/10.1007/s00170-021-06630-5.
[60] Chen L, Peng S, Liu J, Liu H, Chen L, Du B, et al. Compressive response of multi-layered thermoplastic composite corrugated sandwich panels: modelling and experiments. Compos Part B Eng 2020;189:107899. https://doi.org/10.1016/j.compositesb.2020.107899.
[61] Romanenko V, Duhovic M, Schommer D, Hausmann J, Eschl J. Advanced process simulation of compression molded carbon fiber sheet molding compound (C-SMC) parts in automotive series applications. Compos A: Appl Sci Manuf 2022;157:106924. https://doi.org/10.1016/j.compositesa.2022.106924.